JOURNAL OF GEOPHYSICAL RESEARCH, VOL. 102, NO. E12, PAGES 28,705–28,716, DECEMBER 25, 1997

Laser Raman spectroscopy of varnished basalt and implications for in situ measurements of Martian rocks

Elisa J. Israel, Raymond E. Arvidson, Alian Wang,
Jill D. Pasteris, and Bradley L. Jolliff

Department of Earth and Planetary Sciences and McDonnell Center for the Space Sciences, Washington University, St. Louis, Missouri

Abstract. Earth-based and orbital spectroscopy and Viking Lander data strongly suggest that rocks on Mars are coated with indurated dust deposits. Rock coatings will influence mineralogical measurements to be acquired in situ from Mars rovers and other surface missions, in that most techniques will detect the coatings and/or coatings plus underlying minerals. In this paper, we present results of experiments on varnished basalt cobbles from the Lunar Crater Volcanic Field, Nevada, using laser Raman spectroscopic microprobe measurements obtained with a 514.5 nm Ar^+ laser and irradiation spot sizes from 1 to 20 μm. Measurements from thin sections and fresh, unprepared rock surfaces clearly allow identification of igneous minerals. Varnish spectra acquired from thin sections as well as from unprepared exterior rock surfaces typically show broad peaks consistent with the fine-grained nature of varnish and the dominance of manganese oxide and clay minerals. Several areas also show sharp Raman peaks due to phosphates and anatase, indicative of the heterogeneity of varnish deposits. Raman spectra taken through varnished rock surfaces reveal the mineralogy of coatings (where varnish is >15 μm in thickness) and a combination of coatings and igneous minerals in areas with thinner varnish. Given the abundance of rock coatings observed at the Viking and Pathfinder landing sites, results indicate that techniques such as Raman spectroscopy (and any others with comparable penetration depths) will sample some combination of coatings and underlying rock materials. The ability to make many in situ measurements across samples, coupled with the ability to expose fresh rock surfaces, will be needed to unambiguously characterize both the coatings and the rocks on Mars from future landers and/or rovers.

1. Introduction

The Mars Surveyor Program includes rovers to be launched in 2001 and 2003. A key objective of the rover missions will be in situ measurements of rock and soil mineralogy and collection of samples for return during the 2005 mission. Rocks are particularly important targets for analysis, since they may represent local geological processes (e.g., hydrothermal deposits or ancient lake bed strata) (Figure 1). The presence of coatings on Martian rocks is indicated by Earth-based reflectance spectra [*Singer*, 1980; *Singer and Roush*, 1983; *McCord et al.*, 1982] Varnish consists primarily of manganese oxides (most commonly birnessite), iron oxides (typically hematite), and illite-montmorillonite clays [*Potter and Rossman*, 1977]. Most researchers believe that the Mn-oxide-rich material is affixed to the rock surface by bacteria and/or fungi [*Dorn and Oberlander*, 1981; *Krumbein and Jens*, 1981; *Taylor-George et al.*, 1983; *Nagy et al.*, 1991].

For background, LRMS uses monochromatic radiation (i.e., a laser) as excitation and collects the radiation scattered from samples. The frequency of the scattered radiation is shifted

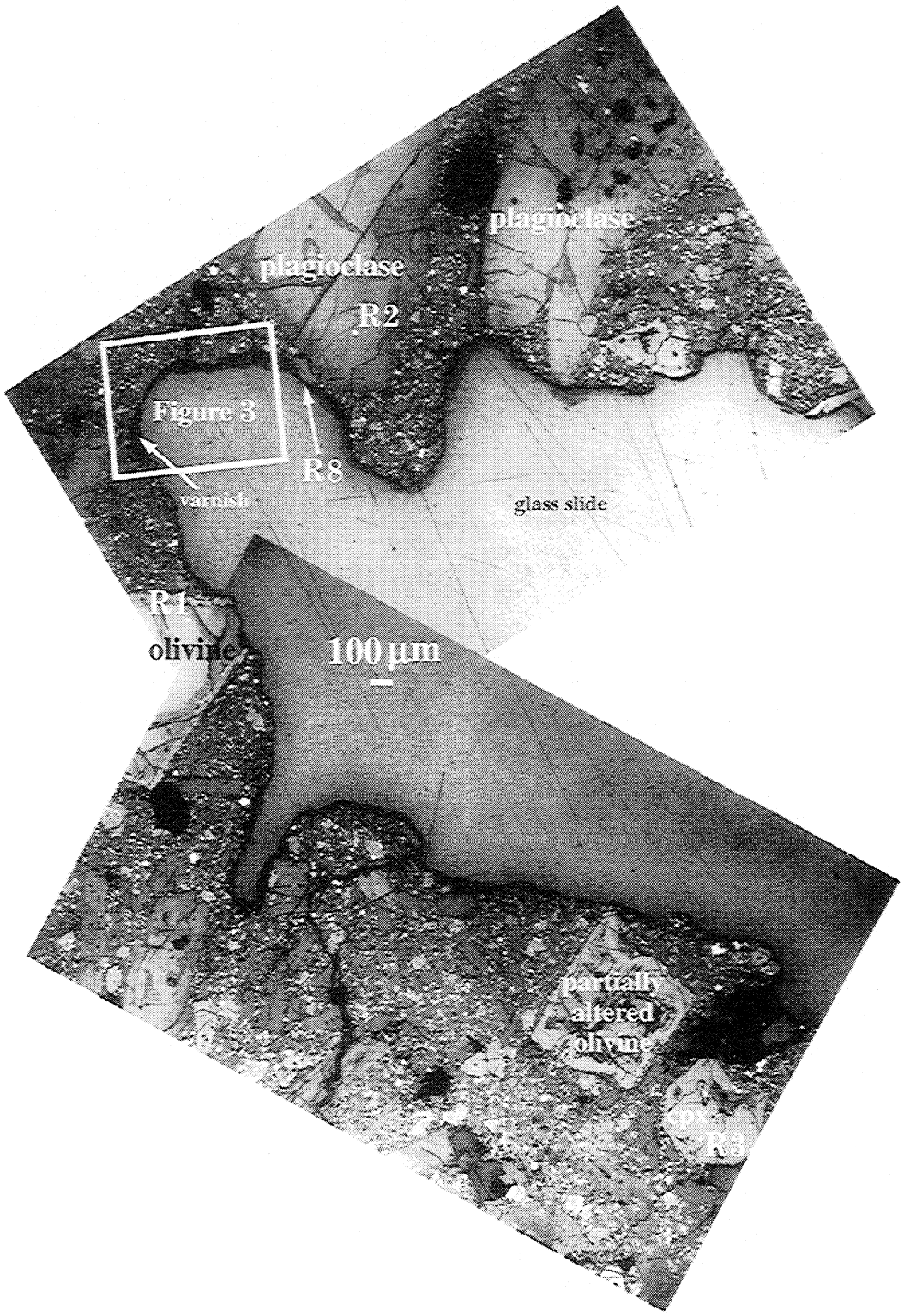

Figure 2. Photomicrographs in reflected light of the area of thin section QBV-B3 from which many of the Raman spectra were taken. Varnish is prevalent along much of the outer edge of the rock as a dark band of varying thickness in sharp contact with the underlying rock. Characteristic minerals are noted, as is the location of Figure 3. Points labeled R1, R2, R3, and R8 represent locations for which Raman spectra were obtained. Points R1, R2, and R3 were acquired with the thin section lying flat and correspond to spectra shown in Figure 6. Point R8 (indicated by an arrow representing the direction of the laser) marks the approximate location for spectra (Figure 7d, Figure 10a) obtained with the thin section propped on edge.

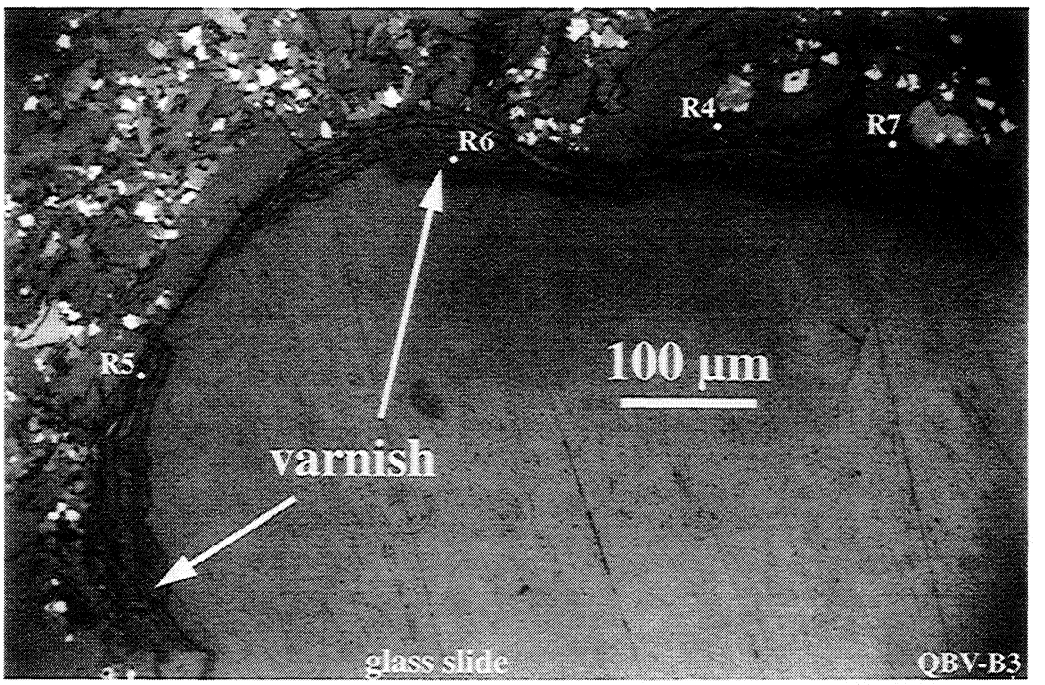

Figure 3. Photomicrograph of a portion of thin section QBV-B3 in reflected light. Thickest varnish in this region is ~60 μm. The points labeled R4, R5, R6, and R7 represent locations from which Raman spectra were obtained, as shown in Figures 6, 7, and 9.

ence of clays, Mn-oxides, and apatite [*Israel*, 1996]. Comparisons of the oxide abundances of the varnish with those of several minerals considered likely to be present in the varnish provided additional mineralogical information [*Israel*, 1996].

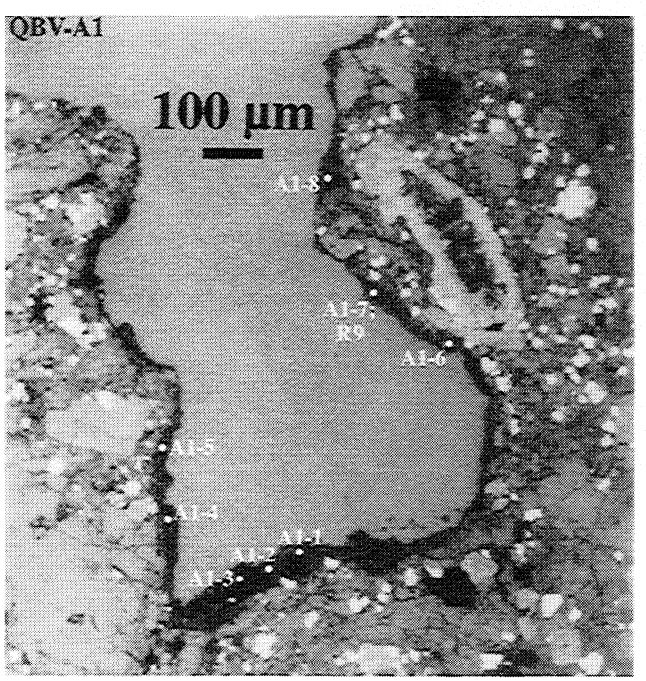

Figure 4. Photomicrograph of thin section QBV-A1 taken in reflected light. Points labeled A1-1 through A1-8 represent the eight electron microprobe sample points (data in Table 1) for this region. A Raman spectrum (Figure 10b) from this region was obtained from the area near point A1-7 and is labeled R9. The vug-like depression depicted in this photomicrograph (whole vug not visible at this magnification) is ~2 mm deep. The thickest varnish is ~90 μm.

These results indicate that the Mn-oxide component is likely a mixture of pyrolusite (MnO_2) and romanechite ($BaMn^{2+}Mn_8^{4+}O_{16}(OH)_4$) and that birnessite ($Na_4Mn_{14}O_{27} \cdot 9H_2O$), common in other varnishes [*Potter and Rossman*, 1979], is probably not present in the varnish on this sample. The strong correlation between SiO_2 and Al_2O_3 concentrations is consistent with the presence of a clay mixture consisting of ~31% illite and ~69% montmorillonite. Additionally, a positive correlation between CaO and P_2O_5 indicates the presence of apatite ($Ca_5(PO_4)_3(F,Cl,OH)$).

3. Raman Measurements

3.1. Overview

The LRMS instrument used for these experiments is an S3000™ micro-Raman spectrometer manufactured by the Instruments SA/Jobin-Yvon company. It has a 1 m focal length spectrograph (600 g/mm holographic grating, Czerny-Turner configuration, $f/5$), coupled with two subtractive premonochrometers ($f/7.5$). An intensified diode array (1024 pixel) is used as a multichannel detector, and the 514.5 nm line of an Ar^+ laser as the excitation source. The LRMS measurements in this study were performed by using the microsampling system of this spectrometer. The hand samples of the rock and the thin sections were placed on a microscope stage and irradiated by the excitation laser beam focused through a microscope objective. The same objective was used to collect the scattered Raman radiation from the samples. The 80× ultralong working distance microscope objective used to collect most of the Raman spectra presented in this paper has a numerical aperture of 0.75 and thus provides a relatively high collecting efficiency of the scattered Raman radiation (corresponding to a collecting solid angle of 0.677π steradians).

Two types of LRMS measurements were obtained. Type I measurements were performed on the thin sections of the rock

Figure 5. Photomicrograph of thin section QBV-A2 taken in reflected light. Labeled points represent the six electron microprobe sample points for this region. These correspond to data with the prefix A2 in Table 1. Varnish thickness ranges from ~7 to 35 μm.

sample with the plane of the thin section either perpendicular or parallel to the incident laser beam. Type II measurements were acquired directly from the cobble surfaces with the laser impinging at a 0° incidence angle onto varnished and fresh, broken surfaces. The only sample treatment used for Type II measurements was ultrasonic cleaning in acetone to remove the contamination by human handling.

3.2. Type I Host Rock Measurements

The interior of section QBV-B3 was examined using LMRS, including regions with phenocrysts and mesostasis. Figure 6 shows Raman spectra of olivine, plagioclase, and clinopyroxene obtained from the phenocrysts in thin section QBV-B3. The sampling locations for spectra in Figures 6a–6d and 6f are marked on Figures 2 and 3 as points R1, R2, R3, and R4. The sampling location for the spectrum in Figure 6e is not pictured here but was also on the same thin section as those for the spectra in Figures 6a–6d and 6f. These characteristic spectra with their sharp nonoverlapping peaks and high signal-to-noise ratio illustrate the capabilities of LMRS for unambiguous mineral identification. Each igneous mineral is easily distinguished from others, making possible the identification in a single spectrum of both feldspar and clinopyroxene in mesostasis (Figure 6d).

Characteristic olivine spectra (Figure 6a) were obtained from a few unaltered olivine grains and from the unaltered regions of altered iddingsite olivine grains. The olivine doublet in the 800–900 Δcm^{-1} spectral range is due to the coupling of symmetric stretching and bending vibrations of the SiO_4 group in the olivine structure [*Iishi*, 1978; *Piriou and McMillan*, 1983; *Servoin et al.*, 1972 in *Griffith*, 1975]. Plagioclase grains show characteristic Raman spectra (Figure 6b). The main features (the strong double peaks near 505 Δcm^{-1} and 484 Δcm^{-1}) are produced by the motion of oxygen atoms along a line bisecting the T-O-T angle (where T = Si or Al) in its structure [*Sharma et al.*, 1983]. Characteristic pyroxene spectra were obtained from phenocrysts and mesostasis areas (Figures 6c and 6d). The spectral pattern and the peak positions (series between 300 and 400 Δcm^{-1}, ~670 Δcm^{-1}, ~1000 Δcm^{-1}) of these spectra suggest that these pyroxene grains mostly have a monoclinic structure [*Delé-Dubois et al.*, 1980; *Wang et al.*, 1995]. Peaks for hematite (Figure 6e) are detected following alteration of an iddingsite grain by laser heating. A very sharp extra peak near 960 Δcm^{-1} appears in the Raman spectrum (Figure

Table 1. Compositions of Desert Varnish by Electron Microprobe Analysis

	SiO_2	TiO_2	Al_2O_3	FeO	MnO	MgO	BaO	CaO	Na_2O	K_2O	P_2O_5	Sum
A1-1	45.1	2.76	19.4	7.36	3.52	3.72	0.46	1.34	0.12	2.97	0.33	87.1
A1-2	44.6	1.20	17.9	7.90	3.59	3.45	0.39	1.85	0.14	3.13	0.66	84.9
A1-3	45.0	1.06	19.0	8.09	2.65	3.65	0.30	1.63	0.19	2.87	0.38	84.9
A1-4	45.7	0.57	21.0	6.97	1.42	3.76	0.28	3.32	0.12	2.88	1.75	87.7
A1-5	26.9	0.30	12.7	5.79	1.12	2.14	0.19	21.83	0.08	1.76	14.02	86.9
A1-6	33.9	0.62	15.8	7.79	2.09	2.52	0.35	14.09	0.14	2.57	8.78	88.6
A1-7	27.8	0.45	13.7	6.45	1.29	2.09	0.18	20.03	0.13	2.05	12.79	86.9
A1-8	31.2	0.77	14.2	6.63	9.27	2.48	1.54	9.93	0.11	2.32	6.48	85.0
A1 average	37.5	0.97	16.7	7.12	3.12	2.98	0.46	9.25	0.13	2.57	5.65	86.5
A2-1	27.2	0.38	15.7	8.11	23.28	2.76	2.48	1.38	0.05	0.76	0.57	82.6
A2-2	29.4	0.44	14.3	6.97	23.44	2.46	3.03	1.05	0.13	0.94	0.51	82.7
A2-3	24.2	0.39	12.4	11.37	24.93	2.07	1.86	1.48	0.08	0.52	1.08	80.8
A2-4	34.9	1.05	16.1	10.65	13.01	2.59	1.20	1.05	0.12	2.13	0.63	83.3
A2-5	32.7	0.54	16.2	8.56	17.82	2.51	1.33	0.86	0.04	0.68	0.57	81.8
A2-6	30.6	0.73	14.4	8.37	20.61	2.57	2.18	0.95	0.04	0.80	0.64	81.8
A2 average	29.8	0.59	14.8	9.01	20.52	2.49	2.01	1.13	0.08	0.97	0.67	82.2
Mean	34.2	0.80	15.9	7.93	10.57	2.77	1.13	5.77	0.11	1.88	3.51	84.6

Oxide concentrations (in wt %) of varnish from thin sections QBV-A1 and QBV-A2 are shown. For each thin section the data points all lie within close proximity to each other (Figures 4 and 5). Labels beginning with A1 indicate one of the eight samples obtained from thin section QBV-A1, while those beginning with A2 indicate one of the six samples obtained from QBV-A2. The low sums are most likely due to the high porosity of the varnish and the presence of structural or adsorbed water, which we have not measured. Electron microprobe spot size is 5 μm.

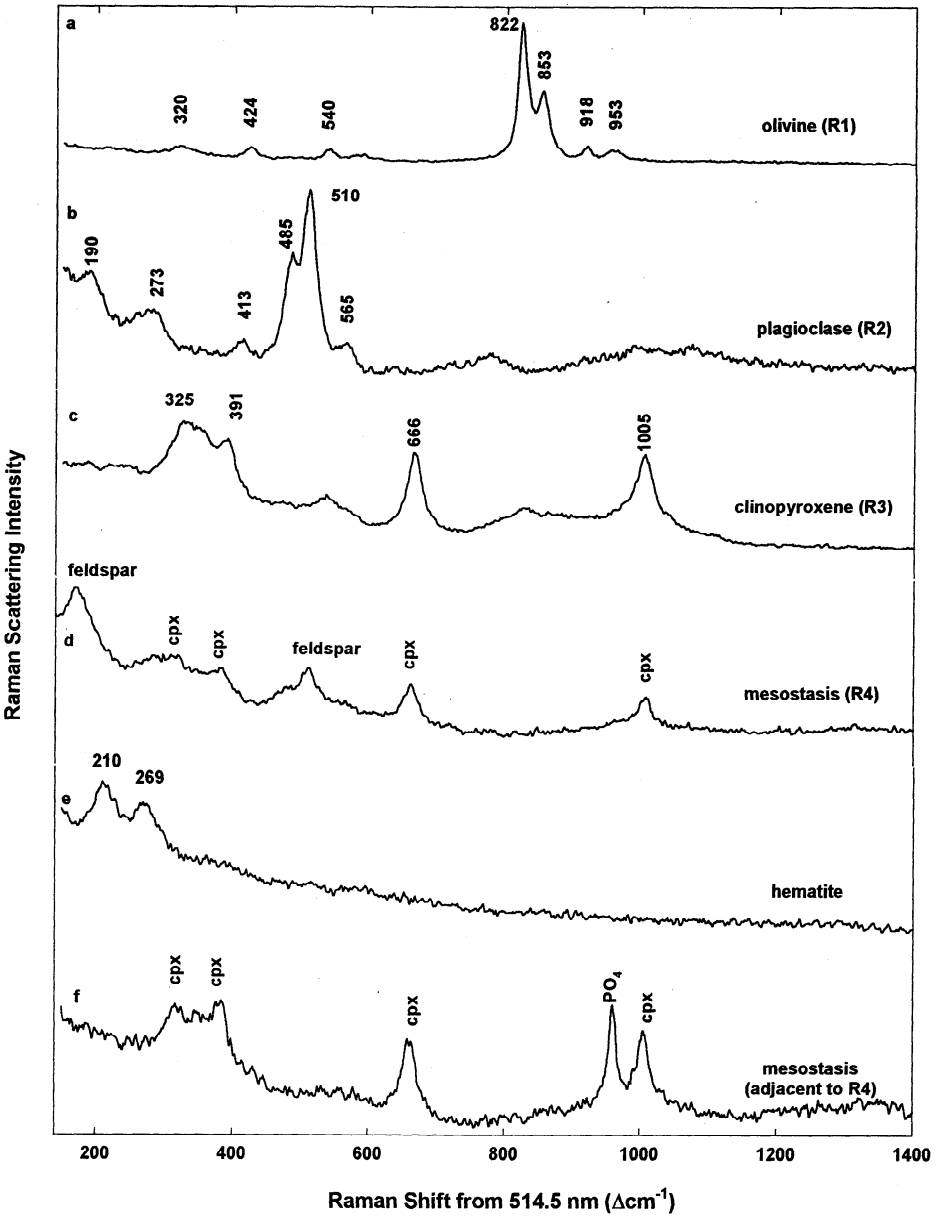

Figure 6. Raman spectra of several characteristic minerals of the basalt cobble, measured from thin section QBV-B3 using the 80× objective (~1 μm beam diameter), laser power (P) ~15 mW at the sample surface, and measurement time (t) < 1 min: (a) unaltered olivine (point R1, Figure 2); (b) plagioclase (point R2, Figure 2); (c) clinopyroxene (point R3, Figure 2); (d) mesostasis area showing a mixture of clinopyroxene and feldspar (point R4, Figure 3); (e) iddingsite grain altered by laser heating, showing hematite peaks; (f) a euhedral clinopyroxene grain at boundary of host rock and varnish coating, showing an extra peak, apparently from apatite (adjacent to point R4, Figure 3).

6f) obtained in the vicinity of a small euhedral clinopyroxene grain, located at the contact between mesostasis and a varnish layer. The position of this peak implies the existence of apatite, a calcium phosphate whose strongest peak (symmetric stretching vibrational mode of PO_4 tetrahedron) occurs near this frequency. The other weak peaks of apatite near 580 and 430 Δcm^{-1} may be obscured by the relatively noisy background in these regions of this spectrum.

3.3. Type I Varnish Measurements

3.3.1. Overview. Raman spectra of the varnish were taken on the flat, polished surface of thin sections QBV-B3 and QBV-A1 and from thin section QBV-B3 as it was supported on edge. In total, over 100 Raman analyses were made on areas of different textures and relative brightnesses under reflected light. This paper contains the most characteristic and/or most informative spectra of those obtained. Thin section QBV-B3 was transferred from its original glass slide to an aluminum plate in order to avoid interference from the Raman peaks of the glass slide and the mounting epoxy. With the thin section lying flat on the aluminum plate (which offers no Raman peak), Raman spectra were obtained from the unlayered varnish regions (lower left part of Figure 3) as well as from the individual layers (upper parts of Figure 3) observed in the

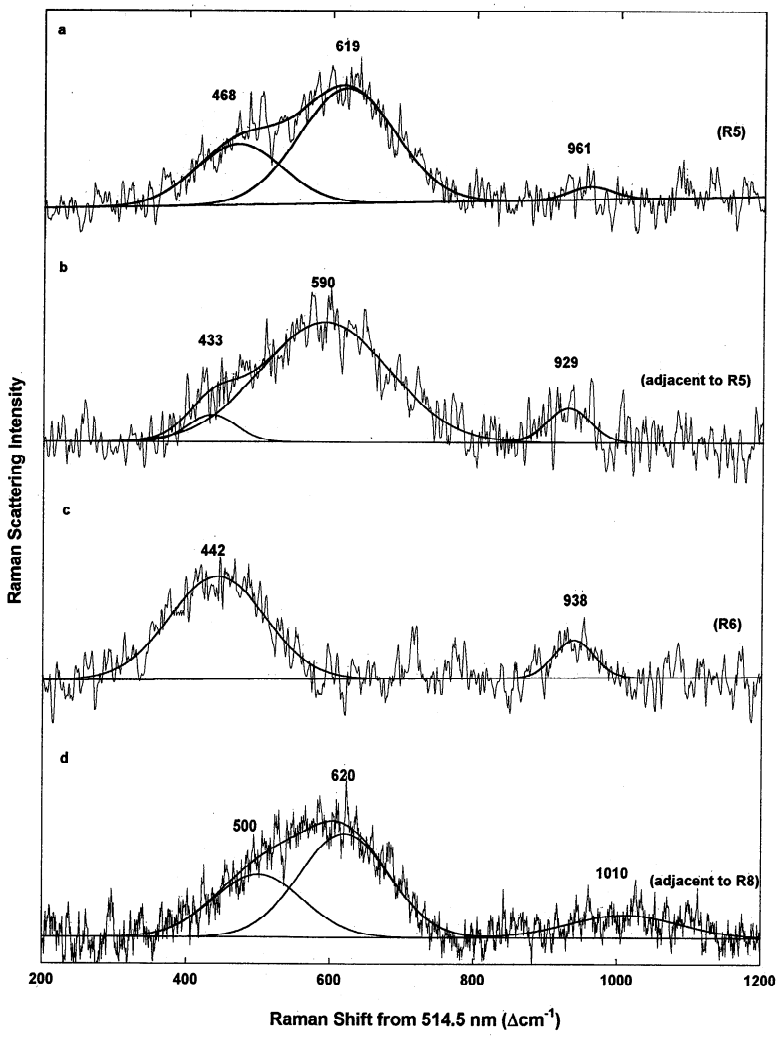

Figure 7. Type I Raman spectra of varnish measured on thin section QBV-B3. (a–c) Spectra were measured with the plane of the thin section perpendicular to the incident laser beam, using an 80× objective: (a) a dark band in layered varnish (point R5, Figure 3) ($P < 2$ mW, $t \sim 1.5$ min); (b) a lighter band in layered varnish (adjacent to point R5, Figure 3) ($P < 2$ mW, $t \sim 1.5$ min); (c) varnish area altered by laser heating (point R6, Figure 3) ($P \sim 7$ mW, $t \sim 1$ min). The spectrum in Figure 7d was measured with the varnished edge of the thin section (i.e., the original varnished surface of the rock) normal to the incident laser beam. The measurement was done in a surface area that appears black in reflected light (adjacent to point R8, Figure 2) ($P < 2$ mW, $t \sim 3.5$ min). Note that the vertical scale has been increased by several-fold relative to data shown in Figure 6 to better illustrate the subtle features associated with varnish spectra. Curve-fitting analyses were done on these spectra using the Grams/386 curve-fitting program. The spectral deconvolution uses a Gaussian-Lorentzian mixed line shape with a free-constraint-fit calculation, meaning that all four spectral parameters for each peak (position, width, height, and shape) as well as the two parameters for a linear-baseline background (slope and intersection) were adjusted after each iteration without any constraint until a convergence was reached. The number of peaks is selected and tested interactively to achieve a best fit.

thicker varnish areas. Both narrow (~1–3 μm diameter, 80× objective) and broad (~3–9 μm diameter, 20× objective) laser beams and a range of laser powers (~0.1–10 mW at the sample surface) were employed. Spectral noise was generally higher farther from the rock-varnish interface and in the area of unlayered varnish. Additional Raman spectra were taken in the varnish coating from section QBV-A1 near points analyzed with the electron microprobe.

Acquisition of spectra from the varnished edge of a thin section was also done on section QBV-B3. The section was cut and mounted such that the laser beam could probe into the edge of the sample at 0° incidence angle at points where the varnish thickness was known through petrographic microscope observations and photomicrographs. Figure 3 and the area just to the right of that figure (see Figure 2 for a broad-scale image) show the areas of interest. The majority of the spectra were obtained with a narrow laser beam because the broad laser beam induced a high fluorescence background that precluded acquisition of informative spectra. Laser power ranged from ~0.1 to 10 mW at the sample surface.

The most common LRMS spectral pattern for the varnish contains a broadband near 600 Δcm^{-1} and a weak band ~900–1000 Δcm^{-1} that are not immediately identifiable as specific minerals (Figure 7). The deconvolution of these spectra shows

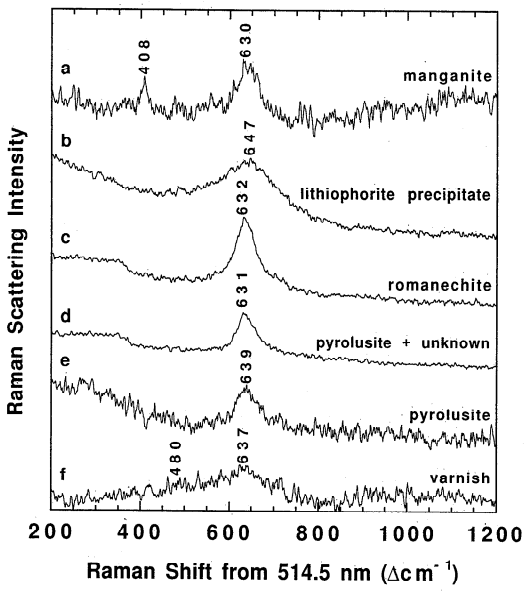

Figure 8. Raman spectra of several Mn-oxide standards, from the research mineral collection in the Department of Earth and Planetary Sciences at Washington University and confirmed by X ray diffraction analyses. They are (a) manganite, γ-MnO(OH); (b) lithiophorite, $(Al,Li)MnO_2(OH)_2$; (c) romanechite, $BaMn_9O_{16}(OH)_4$; (d and e) pyrolusite, MnO_2. A varnish spectrum (Figure 8f) obtained from the surface of the basalt cobble (QBV-A) is shown for comparison.

that the broadband near 600 Δcm^{-1} is not symmetric and is best fit by two bands: one in the 400–500 Δcm^{-1} range and one in the ~620–630 Δcm^{-1} range. The curve fit also makes the third, comparatively weak band, centered in the 900–1000 Δcm^{-1} region, more readily identifiable.

The fine-grained and chemically heterogeneous nature of the varnish influences its Raman spectral properties, for instance, causing weak, broadbands with variable central frequencies. Raman scattered radiation is produced by dipole emission induced by the electromagnetic field of the excitation laser. It thus is a volume-scattering process. Decreasing grain size reduces the volume to surface ratio, and increasing porosity reduces the ratio of occupied to unoccupied space in the volume irradiated by a focused laser beam. Both effects reduce the total number of molecules in the irradiated volume, thus reducing the number of Raman photons produced within the irradiated volume. The loss of long-range order in the crystal structure (decrease of crystallinity) causes Raman peak broadening due to contributions from slightly different vibrational units, accompanied by the reduction of peak intensities and shifts of peak positions. Multiple reflections at various boundaries within the sampled material are also an important control on the magnitude of the Raman effect due to scattering and absorption. Thus for the varnish spectra the typical weak Raman bands could be explained as a combined result of low productivity of Raman photons and high losses in throughput. The large bandwidths actually could be the overlapping of different Raman peaks contributed by slightly different (chemically or structurally) vibrational units in the irradiated volume.

3.3.2. Manganese oxide minerals. Figure 8 illustrates the Raman spectra of Mn oxides that have spectral features similar to those found in the varnish spectra. Spectra in Figures 8a–8e were obtained from a pyrolusite, a mixed sample of romanechite interleaved with manganite bands, a pyrolusite mixed with an unidentified mineral, and a fine-grained precipitate of lithiophorite ($(Al,Li)MnO_2(OH)_2$) on a chert sample. The main peak for all of these samples lies in the 630–650 Δcm^{-1} range, which is similar to the central position for the dominant component band of the varnish band near 600 Δcm^{-1} (Figure 8f). Based on peak position, romanechite, pyrolusite, and manganite are all possibilities. Romanechite and pyrolusite are more likely than manganite because the manganite spectrum also contains a peak at 408 Δcm^{-1}, which is not observed in any of the varnish spectra. However, a peak at that position in the varnish spectra may be lost in the background noise, so manganite cannot be completely discounted. The fact that the position of this component band varies somewhat between different varnish spectra suggests a combination of more than one Mn-oxide, possibly romanechite and pyrolusite, the relative amounts of which may vary from place to place within the varnish. This is consistent with the overall heterogeneity of varnish composition.

Aside from peak position, the other noticeable characteristic of the main varnish band is its width. The standards with main peak positions most similar to that of the varnish (pyrolusite, manganite, and romanechite), all have much sharper peaks than the varnish. Only the fine-grained lithiophorite precipitate shows a much broader peak. Although the position of the lithiophorite peak is at a higher wavenumber than those observed in the varnish and thus indicates that lithiophorite is not present in the varnish, the width of the peak is indicative of the precipitate's fine grain size. The same inverse correlation may hold between peak width and grain size in the varnish.

3.4. Cryptocrystalline Materials

As discussed earlier, the most common Raman spectra detected from varnish are typified by two very broad bands in 450–650 and 950–1050 Δcm^{-1} spectral regions (Figure 7). The component band in the 590–640 Δcm^{-1} region of the first band has been attributed to Mn-oxides in the previous discussion. The component band in the 450–550 Δcm^{-1} range of the first band and the much weaker second band in the 950–1050 Δcm^{-1} high-frequency region will be discussed in this section. These two bands are intrinsically related to each other because they coexist in most spectra, including a spectrum that shows no evidence of the Mn-oxide feature (Figure 7c). The locations of these two bands suggest that they are due to silicates. The width and weakness of the band suggest that they are cryptocrystalline and/or very fine grained minerals (e.g., clays). The presence of phyllosilicate clays is suggested mainly by the Q-mode factor analysis using the electron microprobe data for varnish, and by previous studies of desert varnish. In general, clay minerals show weak Si-O_{nb} stretching vibrational bands in the 700–1200 Δcm^{-1} range, a stronger band of Si-O_b-Si symmetric vibration in the 700–600 Δcm^{-1} range, and many bands related to lattice modes below 500 Δcm^{-1}. Montmorillonite, for example, shows peaks near 520 and 700 Δcm^{-1} [*Herman et al.*, 1985]. However, when grain sizes are extremely small, as in a finely powdered sample, Raman peaks are weak and easily obscured by spectral features of other minerals or by fluorescence. Although clays generally have characteristic Raman peaks in the 3500–4000 Δcm^{-1} region (OH stretching vibrational modes), they were not observed in the measurements done on this varnish, possibly for the same reasons. However, the fact that the Raman peaks of clay minerals are not observed in the spectra of varnish does not mean that they are not

present, simply that they may be masked. It is also possible that the characteristic Si-O_b-Si vibration of some clay minerals (located at 633 Δcm^{-1} for kaolinite) are blocked by the broadband of Mn-oxides in the 590–640 Δcm^{-1} region.

3.4.1. Anatase. Anatase (TiO_2) was identified in several locations within the varnish by the main anatase peak near 148 Δcm^{-1} [*Beattie and Gilson*, 1968 in *Griffith*, 1975]. Figure 9a (point R7, Figure 3) shows a typical varnish spectrum, characterized by the broad Mn-oxide band. This spectrum, obtained with a low-magnification (20×), low numerical aperture objective, and thus a large spot size, also clearly shows the main peak for anatase. When the same area was analyzed with the 80×, large numerical aperture objective (small spot size), a sharp spectrum for anatase alone was observed (Figure 9b), without evidence of the low signal-to-noise ratio and broadbands typical of varnish. Anatase was not detected in the matrix of the rock. The anatase in the varnish may be detrital material deposited in the varnish or it may have developed because of oxidation of ilmenite near the rock surface. It may also be associated with the clays whose presence is suggested by the electron microprobe analyses.

3.4.2. Apatite. As discussed earlier, the electron microprobe results suggest the presence of a Ca-phosphate phase in some areas of the varnish. High CaO and P_2O_5 concentrations, in the correct proportions for apatite, were measured on thin section QBV-A1 in a deep vug-like depression at points A1-5, A1-6, A1-7, and A1-8 (Table 1) as marked in Figure 4. These areas were reexamined with the laser Raman microprobe to determine if an apatite-like phase could be detected in the same areas. Pure apatite normally produces a distinctive Raman spectrum with its main peak near 963 Δcm^{-1} due to the symmetric stretching vibration of the (PO_4) tetrahedron. The peak position can shift depending on the exact composition of the phase as shown for the apatite spectrum in Figure 10 [*Kravitz et al.*, 1968 in *Griffith*, 1975]. Spectra from the varnish (point R8, Figure 2; point R9, Figure 4), showing peaks at 957 and 955 Δcm^{-1}, respectively, are shown for comparison. In the spectrum in Figure 10a, both this main peak and a smaller peak at 418 Δcm^{-1} correlate approximately with peaks in the apatite spectrum, indicating the presence of a Ca-phosphate (likely apatite) in the rock coating. The spectrum in Figure 10a was obtained from the varnished edge of thin section QBV-B3 when it was oriented edge-on. This spectrum was recorded with high laser power (~10 mW at the sample surface) following a series of spectral acquisitions for which we purposely allowed the laser to alter the varnish. It is possible that by "burning off" the low-temperature minerals, we removed enough material to isolate an apatite grain, but we did not penetrate the varnish at this spot because we did not obtain a signal for plagioclase which was present at the rock-varnish contact. Under the conditions of this experiment (laser wavelength and varnish mineralogy), a 15 μm thick layer of varnish (Figure 2) prevented detection of the underlying mineralogy. The Ca-phosphate signature also was detected from within the varnish on thin section QBV-A1 (point R9, Figure 4). This spectrum (Figure 10b) also was obtained after the laser had damaged the sample surface. In both cases in which the Ca-phosphate signature was detected in varnish coatings, the broad Mn-oxide band was not observed. This observation is consistent with the EMP data showing that regions with high CaO and P_2O_5 concentrations have low MnO concentrations

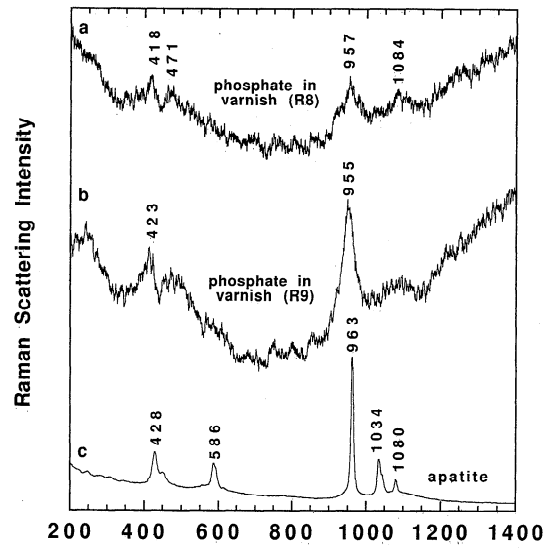

Figure 10. Type I Raman spectra of varnish measured on thin sections QBV-B3 and QBV-A1. (a) Spectrum (point R8, Figure 2) was measured on a light colored area with the edge of thin section QBV-B3 (i.e., the original varnished surface of the rock) normal to the incident laser beam (80× objective, $P \sim 15$ mW, $t \sim 2.5$ min). The sampling site was damaged by laser heating. (b) Spectrum (point R9, Figure 4) was measured from thin section QBV-A1 with the plane of the thin section perpendicular to the incident laser beam (80× objective, $P \sim 10$ mW, $t \sim 20$ s). This sample site also was damaged by laser heating. (c) Characteristic Raman spectrum of apatite (measured by B. Wopenka) is shown for reference.

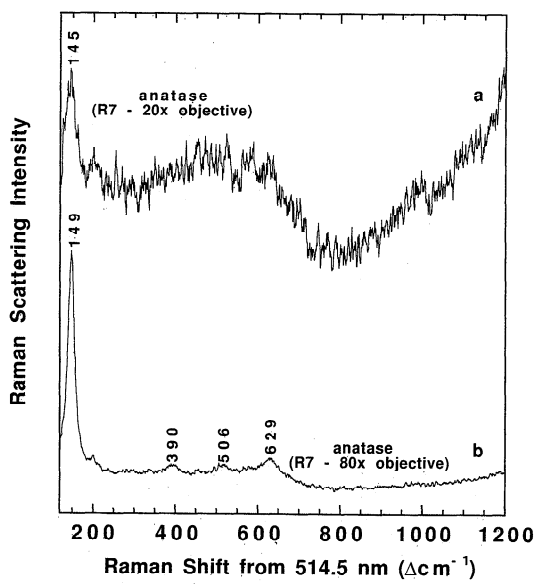

Figure 9. Type I Raman spectra of varnish measured on thin section QBV-B3, showing the presence of anatase (TiO_2) in the varnish. (a) Spectrum (point R7, Figure 3) was obtained using a 20× objective with the plane of the thin section perpendicular to the incident laser beam ($P \sim 7$ mW, $t \sim 3.3$ min). A sharp peak at 145 Δcm^{-1} is the main characteristic Raman peak of anatase, whereas the accompanying broadband near 600 Δcm^{-1} suggests Mn-oxides. (b) Spectrum was measured at the same location, but using an 80× objective ($P \sim 7$ mW, $t \sim 1.3$ min). It is a characteristic Raman spectrum of anatase [*Beattie and Gilson*, 1968 in *Griffith*, 1975].

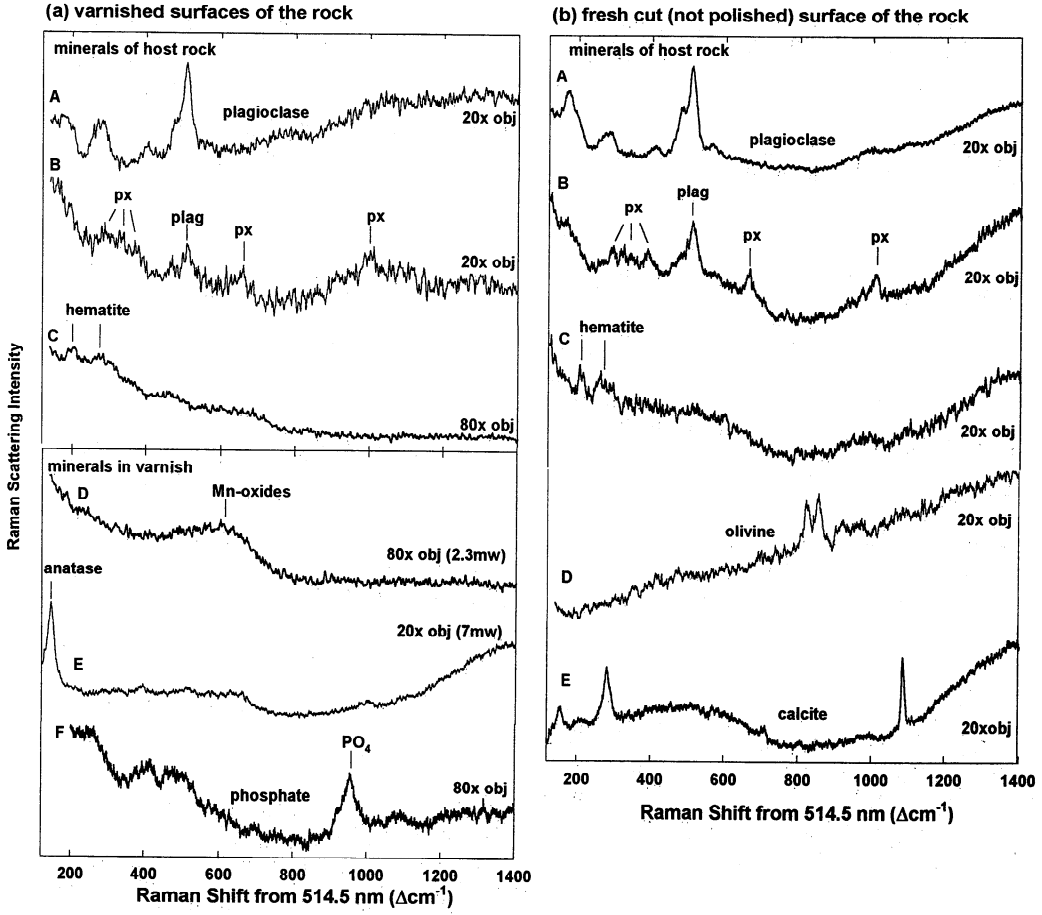

Figure 11. Type II Raman spectra. (a) Spectra were obtained directly from varnished surfaces of the hand sample of basalt. The objective used in the measurements is indicated with each spectrum; laser power at the sample is about 15 mW unless marked otherwise. Measurement times ranged from 0.5 to 3.5 min depending on the sampling sites. (b) Spectra were obtained directly from a fresh cut (not polished) surface of the hand sample of the rock. A 20× objective was used for all these measurements, with laser power about 7 mW at the sample and measurement times ranging from 1.5 to 5 min. See text for details.

and provides further indication of the heterogeneous nature of desert varnish.

3.5. Type II Raman Measurements

The unprepared varnished surface of hand sample QBV-A was analyzed directly with the Raman microprobe by positioning the hand sample on the microscope stage and irradiating it with the condensed laser beam. Given the laboratory-based equipment used, this configuration most closely simulates how Raman spectra would be obtained on Mars. Spectra were obtained from a variety of sample sites including local depressions and areas with locally high relief as well as areas that appeared either visually dark or light in color. Both narrow (~1–3 μm diameter) and broad (~3–9 μm diameter) laser beams were used with laser powers ranging from ~1.5 to 10 mW at the sample surface.

Figure 11a shows a set of typical Raman spectra obtained from these unprepared varnished rock surfaces. For comparison, spectra for a fresh cut surface are shown in Figure 11b. The varnish minerals identified from Type I measurements all are present in the Type II data (spectra D, E, and F of Figure 11a). In addition, spectra A and B of Figure 11a suggest that plagioclase and pyroxene can be uniquely identified through the varnish, although the signal strength is decreased by an order of magnitude relative to the fresh surface spectra (Figure 11b). We also have obtained some spectra of varnished surfaces that show very weak double peaks of hematite (spectrum C of Figures 11a and 11b), consistent with the presence of iddingsite. Finally, in the measurements done on the fresh cut surface of this rock, spectra of typical minerals of this sample were detected (spectra A, B, C, and D of Figure 11b), as well as a characteristic spectrum of calcite with three strong, sharp peaks, which was obtained from secondary vesicle fillings (spectrum E of Figure 11b).

4. Implications for the Use of Raman Spectroscopy on Mars

Recent developments in optical elements, detectors, and solid-state lasers have made possible the design and construction of small and robust LRMS systems. They are now available for industrial process control. Further, a breadboard model of an LRMS system for Mars rovers is under development in our department [*Wang et al.*, 1997]. Several recent studies have shown that LRMS observations provide information on mineral phases present in rocks and soils [*Wang et al.*, 1995, 1997; *Jolliff et al.*, 1997], mineral proportions in the rocks [*Haskin et al.*, 1997], and compositional information for some

mineral species [*Guyot et al.*, 1986; *Wang et al.*, 1997]. The study reported in this paper is the first use of LRMS to study coated rock samples [*Israel et al.*, 1996, 1997].

Direct evidence for the presence of rock coatings comes from images taken by the Viking Landers [*Guinness et al.*, 1996, 1997a, b]. In forward-scattering geometries, rock surfaces show strong Fresnel reflections, a characteristic common to terrestrial rocks that spall, forming massive surfaces abraded by wind and covered with desert varnish. Similar patterns have been observed in images acquired from the Pathfinder imaging system at Ares Vallis. It must be emphasized that Mars rock coatings are quite distinct in color and albedo from desert varnish. First, the single scattering albedos derived by *Guinness et al.* [1997 and submitted paper, 1997] for varnished basalt from the Pisgah Volcanic Field, California, are typically 0.50. Similar analyses for Viking rocks show that the single scattering albedos are closer to 0.85. Values quoted are for red wavelengths. Single scattering albedos for Mars rocks are similar to values for dust in the Martian atmosphere, implying that the rocks are covered with aerosols. Interestingly, the single scattering albedos of terrestrial atmospheric dust range from 0.7 to 0.9. This implies that terrestrial dust, which is a major varnish contributor, is significantly altered in optical properties during fixation onto rock surfaces. The presence of manganese-fixing bacteria is probably the reason. Apparently, such mineralogical changes are not part of the aerosol coating process on Mars. Finally, we note that exposed rock surfaces were not chipped, spalled, or scraped by the lander arm, even with loads near 10 mPa [*Arvidson et al.*, 1989]. This suggests that dusty rock coatings on Mars are indurated, much like desert varnish.

Raman measurements acquired directly from the varnished surface of samples (from hand sample QBV-A and from thin section QBV-B3 as indicated in Figure 2) approximate the conditions under which spectra would be obtained for Mars rocks. In this situation one must contend with rough surfaces, which makes focusing the laser beam more difficult, as well as the presence of coatings. E. A. Guinness et al. (submitted paper, 1997) show that the skin depth of rock coatings at the Viking landing sites is approximately 20 μm in red wavelengths and less at shorter wavelengths. They suggest that rocks are coated to varying thicknesses, in some cases obscuring underlying materials. With LRMS and other optical techniques it will thus be necessary to examine numerous spots on a rock surface in order to differentiate the mineralogy of the coatings from that of the underlying rock. If, upon analysis of a coated surface, no mineral signatures, or only signatures from the coatings, are detected, it will be necessary to find a fresh surface to investigate host-rock mineralogy. This may involve finding a surface on the sample that lacks coatings or having a mechanism on the rover capable of breaking the rock open so that a freshly cut surface could be analyzed directly.

Acknowledgments. This work was supported by NASA Planetary Geology and Geophysics Program, Goddard Space Flight Center grant NAG5-3870 to Washington University. We thank Dan Kremser for assistance with the electron microprobe analyses, Rex Couture for the XRF analyses, Judd Bowman for figure preparation, Brigitte Wopenka for the Raman spectrum of apatite, and Alan Gillespie for a thoughtful review of the manuscript.

References

Armstrong, J. T., Quantitative analysis of silicate and oxide minerals: Comparison of Monte Carlo, ZAF, and phi-rho-Z procedures, in *Proceedings, 23rd Annual Conference on Microbeam Analysis*, edited by D. E. Newbury, pp. 239–246, San Francisco Press, San Francisco, Calif., 1988.

Arvidson, R. E., J. L. Gooding, and H. J. Moore, The Martian surface as images, sampled, and analyzed by the Viking landers, *Rev. Geophys.*, *27*, 39–60, 1989.

Beattie, I. R., and T. R. Gilson, Single crystal laser Raman spectroscopy, *Proc. R. Soc. London, Ser. A*, *307*, 407–429, 1968.

Delé-Dubois, M. L., P. Dhamelincourt, and H. J. Schubnel, Etude par spectroscopie Raman d'inclusion dans les diamants, saphirs et emeraudes/2. *Rev. Gemmol. A.F.G.*, *64*, 13–16, 1980.

Dorn, R. I., and T. M. Oberlander, Microbial origin of desert varnish, *Science*, *213*, 1245–1247, 1981.

Griffith, W. P., Raman spectroscopy of terrestrial minerals, in *Infrared and Raman Spectroscopy of Lunar and Terrestrial Minerals*, edited by C. Karr Jr., pp. 299–323, Academic, San Diego, Calif., 1975.

Guinness, E. A., R. E. Arvidson, and M. K. Shepard, Specular scattering from rock surfaces at the Viking Lander sites (abstract), *Lunar Planet. Sci., XXVII*, 471–472, 1996.

Guinness, E. A., R. E. Arvidson, M. K. Shepard, and I. Clark, Optical scattering properties of terrestrial varnished basalts compared with rocks and soils at the Viking Lander sites (abstract), *Lunar Planet. Sci., XXVIII*, 491–492, 1997.

Guyot, F., H. Boyer, M. Madon, B. Velde, and J. P. Poirier, Comparison of the Raman microprobe spectra of $(Mg,Fe)_2$, SiO_4, and Mg_2GeO_4 with olivine and spinel structures, *Phys. Chem. Miner.*, *13*, 91–95, 1986.

Haskin, L. A., A. Wang, B. L. Jolliff, R. L. Korotev, K. M. Rockow, and K. V. Viskupic, Laser Raman spectroscopic determination of mineral proportions in rocks on planetary surfaces (abstract), *Lunar Planet. Sci., XXVIII*, 523–524, 1997.

Herman, R. G., C. E. Bogdan, and A. J. Sommer, Laser Raman microprobe study of the identification and thermal transformations of some carbonate and aluminosilicate minerals, in *Advances in Materials Characterization II*, edited by R. L. Snyder, R. A. Condrates, and P. F. Johnson, pp. 113–130, Plenum, New York, 1985.

Iishi, K., Lattice dynamics of forsterite, *Am. Mineral.*, *63*, 1198–1208, 1978.

Israel, E. J., Examination of a desert varnished basalt using electron microprobe analysis and laser Raman spectroscopy, A. M. thesis, Washington Univ., St. Louis, Mo., 1996.

Israel, E. J., R. E. Arvidson, A. Wang, and B. L. Jolliff, New approaches to the in situ study of Martian surface mineralogy (abstract), *Lunar Planet. Sci., XXVII*, 583–584, 1996.

Israel, E. J., R. E. Arvidson, A. Wang, J. D. Pasteris, and B. L. Jolliff, Laser Raman spectroscopic measurements of a desert-varnished basalt and implications for in situ analysis of Martian rocks (abstract), *Lunar Planet. Sci., XXVIII*, 625–626, 1997.

Jolliff, B. L., A. Wang, and L. A. Haskin, Identification of minerals of several Martian surface analog materials by Raman spectroscopy (abstract), *Lunar Planet. Sci., XXVIII*, 675–676, 1997.

Kravitz, L. C., J. D. Kingsley, and E. L. Elkin, Raman and infrared studies of coupled $(PO_4)^{-3}$ vibrations, *J. Chem. Phys.*, *49*, 4600–4610, 1968.

Krumbein, W. E., and K. Jens, Biogenic rock varnishes of the Negev Desert (Israel) and ecological study of iron and manganese transformation by cyanobacteria and fungi, *Oecologia*, *50*, 25–38, 1981.

McCord, T. B., R. N. Clark, and R. B. Singer, Mars: Near-infrared spectral reflectance of surface regions and compositional implications, *J. Geophys. Res.*, *87*, 3021–3032, 1982.

Nagy, B., L. A. Nagy, M. J. Rigali, W. D. Jones, D. H. Krinsley, and N. A. Sinclair, Rock varnish in the Sonoran Desert: Microbiologically mediated accumulation of manganiferous sediments, *Sedimentology*, *38*, 1153–1171, 1991.

Piriou, B., and P. McMillan, The high-frequency vibrational spectra of vitreous and crystalline orthosilicates, *Am. Mineral.*, *68*, 426–443, 1983.

Potter, R. M., and G. R. Rossman, Desert varnish: The importance of clay minerals, *Science*, *196*, 1446–1448, 1977.

Potter, R. M., and G. R. Rossman, The manganese- and iron-oxide mineralogy of desert varnish, *Chem. Geol.*, *25*, 79–94, 1979.

Rivard, B., R. E. Arvidson, I. J. Duncan, M. Sultan, and B. El Kaliouby, Varnish, sediment, and rock controls on spectral reflectance of outcrops in arid regions, *Geology*, *20*, 295–298, 1992.

Servoin, J. L., B. Piriou, and P. Alain, Raman scattering of pure

synthetic forsterite Mg_2SiO_2, *C. R. Hebd. Seances Acad. Sci., Ser. B, 274*, 135–137, 1972.

Sharma, S. K., B. Simons, and H. S. Yoder Jr., Raman study of anorthite, calcium Tschermak's pyroxene, and gehlenite in crystalline and glassy states, *Am. Mineral., 68*, 1113–1125, 1983.

Shepard, M. K., R. E. Arvidson, and E. A. Guinness, Specular scattering on a terrestrial playa and implications for planetary surface studies, *J. Geophys. Res., 98*, 18,707–18,718, 1993.

Singer, R. B., The dark materials on Mars, I, New information from reflectance spectroscopy on the extent and mode of oxidation (abstract), *Lunar Planet. Sci., XI*, 1045–1047, 1980.

Singer, R. B., and T. L. Roush, Spectral reflectance properties of particulate weathered coatings on rocks: Laboratory modeling and applicability to Mars (abstract), *Lunar Planet. Sci., XIV*, 708–709, 1983.

Taylor-George, S., F. Palmer, J. T. Stalet, D. J. Borns, B. Curtiss, and J. B. Adams, Fungi and bacteria involved in desert varnish formation, *Microbial Ecol., 9*, 227–245, 1983.

Wang, A., J. Han, L. Guo, J. Yu, and P. Zeng, Database of standard Raman spectra of minerals and related inorganic crystals, *Appl. Spectrosc., 48*, 959–968, 1994.

Wang, A., B. L. Jolliff, and L. A. Haskin, Raman spectroscopy as a method for mineral identification on lunar robotic exploration missions, *J. Geophys. Res., 100*, 21,189–21,199, 1995.

Wang, A., E. Cortez, and L. A. Haskin, A Raman spectroscopic sensor for on-surface planetary remote sensing (abstract), *Lunar Planet. Sci., XXVIII*, 1489–1490, 1997.

R. E. Arvidson, E. J. Israel, B. L. Jolliff, J. D. Pasteris, and A. Wang, Department of Earth and Planetary Sciences, Washington University, Campus Box 1169, One Brookings Drive, St. Louis, MO 63130-4899. (e-mail: arvidson@wunder.wustl.edu)

(Received June 10, 1997; revised August 19, 1997;
accepted August 28, 1997.)